Picosecond quantum-beat spectroscopy of quadrupole polaritons in Cu_2O

V. Langer, H. Stolz, and W. von der Osten
Fachbereich Physik, Universität-Gesamthochschule Paderborn, Warburger Strasse 100A, 33095 Paderborn, Germany
(Received 31 March 1994; revised manuscript received 19 September 1994)

Quantum beats in picosecond time-resolved resonance fluorescence are investigated in Cu_2O for the yellow $1S$ quadrupole exciton polariton. In order to obtain information on the coherence of the resonant intermediate polariton states, we have studied the electric-dipole allowed light-scattering processes involving one and two Γ_3^- phonons. A quantitative analysis provides exciton-polariton coherence times of about 1 ns at 2 K, decreasing with higher temperatures and larger wave vectors due to phonon scattering. From the magnetic-field dependence, low-field g values are determined with high accuracy. The measurements permit a clear distinction between Raman and hot-luminescence-like contributions to the scattering intensity. The strong effect of the spectral width of the excitation pulse on the time behavior of the scattering, as well as the temperature dependence of the coherence time, indicate that it is essential to take into account the polariton character.

I. INTRODUCTION

Quantum-beat spectroscopy is well known in atomic and molecular physics, mainly as a spectroscopic technique having high resolution to study small energy splittings due to fine and hyperfine interactions (for comprehensive reviews, see, e.g., Refs. 1–3). Recently it was demonstrated that quantum beats also represent a powerful tool to investigate excitonic systems in solids.[4–8] Besides nonlinear methods (see Refs. 9 and 10 and references therein), time-resolved resonant light scattering reported in this contribution was successfully employed to study beating from excitons and can provide valuable knowledge on exciton dynamics.[11,12] The occurrence of the beats originates from the coherent superposition of intermediate states which are closely adjacent in energy and are simultaneously excited by a short optical pulse.

The beating signal provides two important pieces of information. One is the energy splitting of the investigated states which directly follows from the oscillation frequency. Compared with conventional cw measurements in the frequency domain, it can be obtained with much higher spectral resolution and independent of any inhomogeneous broadening. In particular, this is of importance for exciton polaritons because of their intrinsic inhomogeneous broadening due to k-dependent energies. The other information is contained in the damping of the beats which is determined by the coherence time $\tau_{\rm coh}$.[13] It represents the average time during which an ensemble of excited states loses phase information and is related to the homogeneous linewidth of the optical transition by $\delta E_{\rm hom} = 2\hbar/\tau_{\rm coh}$. According to different contributions to the linewidth, the loss rate may be written as

$$\frac{1}{\tau_{\rm coh}} = \frac{1}{2T_1} + \frac{1}{T_2'} \,. \tag{1.1}$$

The first term on the right-hand side takes into account all *inelastic* processes such as radiative recombination, scattering by phonons, or trapping at impurities. T_1 thereby denotes the total *energy relaxation time* (or population lifetime) usually obtained from conventional time-resolved luminescence. The second term involving the *pure dephasing time* T_2' considers all *elastic* processes. They do not lead to a depopulation of the excited states but exclusively affect the phase.

Besides providing energy splittings and all relevant relaxation times, it is even more important that the quantum-beat method allows us to distinguish coherent, i.e., Raman-like, from incoherent or hot-luminescence-like contributions to the emitted intensity. Cu_2O is a well-studied prototype semiconductor for which the low-temperature optical spectrum exhibits rich structure due to excitons (see e.g., Ref. 14). Previous investigations of these excitons by means of resonant light scattering had raised the question as to whether the observed light is due to Raman scattering or to hot luminescence (see Ref. 15, for a survey see Ref. 16). While Raman scattering, in a strict sense, is defined as a process in which the phase coherence of the intermediate state is retained, in hot luminescence the phase coherence is lost. Since quantum beats as an interference effect can only occur in the coherent (Raman) part of the process, our experiments enable us to give an unambiguous answer to this question.

Following a brief description of the experimental equipment in Sec. II, we develop the necessary theoretical basis in Sec. III. In particular we discuss the selection rules for phonon scattering in resonance with the $1S$ quadrupole exciton and derive expressions for the polarized intensities in certain geometries. As we investigate magneto-quantum beats, the splitting and mixing of the states in a magnetic field is considered. Finally a detailed description of the relaxation processes is given affecting the exciton polariton. In Sec. IV we present numerous experimental results and their analysis especially regarding the

polariton character of the exciton that has to be taken into account to obtain a quantitative picture of exciton relaxation in the case of a direct-gap material like Cu_2O. In the appendix we summarize briefly the theory of time-resolved light scattering as needed in the interpretation of the experimental results. Some preliminary results were already published previously.[17]

II. EXPERIMENTAL SETUP

The experimental arrangement to investigate quantum beats is basically that used in conventional time-resolved spectroscopy, however, with the time resolution highly improved.[18] The sample mounted in a magnetic-field cryostat can be excited by nearly transform-limited short laser pulses from a dye laser, synchronously pumped by a mode-locked frequency doubled Nd-doped yttrium-lithium-fluoride laser system with a repetition rate of 76 MHz. Inserting spectral filters with different bandwidths or an additional saturable absorber into the optical resonator of the dye laser we can achieve pulse durations of 0.4–35 ps. With rhodamine 6G as a laser dye the tuning range lies between 570 and 630 nm (2.18 and 1.97 eV).

The transmitted and scattered light was analyzed by means of a 1 m double monochromator with subtractive mounting of the gratings to compensate the light transit-time spread by a single grating and avoid a temporal broadening of the signals. For measuring the time dependence we had available either a system for inverse single photon counting with a fast microchannel plate photomultiplier (Hamamatsu R2566U-07) or a synchroscan streak camera (Hamamatsu C1587), their use depending on the necessary sensitivity and dynamic range. Because of the weak Raman signals, for all measurements presented in the following we took advantage of the higher sensitivity of the photon counting system (about 10^2–10^3 in comparison to the streak camera). In that case, the time resolution, i.e., the system response to a 5-ps laser pulse was at its best 20 ps full width at half maximum. To reduce the zero point jitter along the time scale we directly gave a fraction of the laser pulse via a monomode fiber to the photomultiplier tube. This pulse served as common time reference. To extract the maximum amount of information contained in the time-resolved spectrum, the setup had to be operated transform limited, i.e., with simultaneous optimal spectral and temporal resolution.[18]

An additional beam splitter in the detection beam path imaged a part of the sample surface containing the laser spot on a high sensitivity video camera followed by an image processing system. This allowed us to select an appropriate spot position on the sample and simultaneously guaranteed a high accuracy in reproducing the optical alignment which was particularly important in view of the existence of a zero-field splitting in strained regions of the samples (see below).

For reasons of sample dimension and quality of the various surfaces we used a 0° scattering (transmission) geometry whereby the scattered light was collected within a cone of 6.5°. We have chosen a crystal orientation where the quadrupole transition and, hence, the phonon-assisted dipole transition is allowed. The wave vector of the incident and scattered light were directed along a [001] direction with polarizations along [100] or [110]. The external magnetic field was also applied along [001], i.e. in Faraday configuration ($\mathbf{B} \parallel \mathbf{k} \perp \mathbf{E}$). Even though this geometry requires efficient stray light suppression the advantage in the present case is that the selection rules are simple.

The samples came from the University of Dortmund where they had been cut from high quality natural single crystals and oriented by x-ray diffraction. All measurements were performed by cooling the crystals down to about 2 K in superfluid helium.

III. THE QUADRUPOLE POLARITON

Cu_2O is a semiconductor that exhibits a number of hydrogenlike exciton series (for a review, see e.g., Ref. 14). We investigated the $1S$ exciton of the yellow series, which is formed of an electron from the lowest conduction band (symmetry Γ_6^+) and a hole from the top valence band (Γ_7^+). The exciton is split by the electron-hole exchange interaction into a threefold degenerate Γ_5^+ orthoexciton and a nondegenerate Γ_2^+ paraexciton. Since the conduction and valence bands have the same parity, the $1S$ orthoexciton transition is electric dipole forbidden and only quadrupole allowed. Even though the exciton-photon coupling, due to the quadrupole interaction, is only weak (oscillator strength $f = 3.6\times10^{-9}$; cf. Ref. 19), it leads to a characteristic polariton structure with two branches that represent mixed modes of photon and exciton states. In addition, the quadrupole character leads to a complicated dependence of the oscillator strength on wave vector and light polarization in spite of the cubic symmetry of the material (see e.g., Ref. 20). While for most of the discussion below the exciton picture is sufficient, the analysis of the relaxation behavior requires us to introduce the polariton concept.

A. $1\Gamma_3^-$ and $2\Gamma_3^-$ phonon scattering

To study the coherence properties of the quadrupole exciton state, we have investigated light scattering involving one and two odd parity Γ_3^- phonons [energy $\hbar\Omega(\Gamma_3^-) = 13.6$ meV]. These processes have been studied by various groups both under stationary and pulsed excitation[21–23] and are illustrated in Fig. 1 with the exciton-photon interaction neglected for the time being. One-phonon scattering becomes resonant if the incident laser (at energy E_L) is tuned either directly into the quadrupole transition at $E_Q = 2.0329$ eV [Fig. 1(a); *incoming resonance*] or to the onset of the indirect absorption at $E_Q + \hbar\Omega(\Gamma_3^-)$ [Fig. 1(b); *outgoing resonance*]. In both cases the scattering process involves an electric-quadrupole and a phonon-assisted electric-dipole transition each. Because of the small oscillator strength of the quadrupole transition, enhancement over the nonresonant background occurs only very close to the two

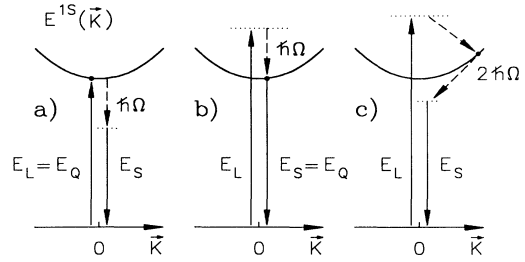

FIG. 1. Schematic representation of the $1S$ orthoexciton dispersion $E^{1S}(\mathbf{K})$ in Cu_2O and considered scattering processes. E_L, E_S, and E_Q are the energies of the incident laser, the scattered photon and the quadrupole exciton, respectively. (a), (b) One-phonon scattering with resonance for the incident and scattered photon. (c) Two-phonon scattering. $\hbar\Omega$: energy of Γ_3^- phonon. The dotted lines represent virtual states.

resonance poles.

Due to the selection rules,[24,25] the scattered intensities are strongly polarized. Making use of the theory of time-resolved light scattering as developed in the appendix (see also Ref. 18) and considering first of all the *incoming* resonance ($E_L = E_Q$), the intensity as function of time of the polarized $1\Gamma_3^-$ phonon Raman process in the exciton picture, where only states at $K = 0$ are taken into account, is given by

$$I^{\mathrm{CS}}(t, \mathbf{e}_L, \mathbf{e}_S) \propto \sum_l \left| \sum_m (\mathbf{M}_m^{\mathrm{EQ}} \cdot \mathbf{e}_L)(\mathbf{M}_{l,m}^{\mathrm{ED}} \cdot \mathbf{e}_S)^* \Psi_m(t) \right|^2 . \quad (3.1)$$

In this equation, $l = 1, 2$ enumerates the two degenerate Γ_3^- phonon modes and $m = 1, 2, 3$ the threefold degenerate Γ_5^+ exciton states. $\mathbf{M}_m^{\mathrm{EQ}}$ and $\mathbf{M}_{l,m}^{\mathrm{ED}}$ are the electric-quadrupole and phonon-assisted electric-dipole transition matrix elements. They can be evaluated by group theory and have to be multiplied by the polarization unit vectors for the incident ($\mathbf{e}_L$) and scattered light ($\mathbf{e}_S$). In Eq. (3.1), the outer summation is performed over the momentum-conserving phonons so that they do not influence the coherence properties of the intermediate exciton states.

Apart from the exciton eigenenergies (E_m) and homogeneous linewidths $\delta E_{\mathrm{hom},m}$, which are assumed to be equal for all states, the scattering amplitude $\Psi_m(t)$ in Eq. (3.1) depends according to Eq. (A7) on the spectral bandwidth and time structure of the excitation pulse and the detection system.[18] While the details of the excitation and the detection process are important when polariton effects are considered (Sec. IV C), for the analysis in the exciton picture it is sufficient to use the white light limit (excitation with a δ-laser pulse and no spectral analysis). In that case the right-hand side of Eq. (A7) reduces to $\exp[-i(E_m - i\,\delta E_{\mathrm{hom}})t/\hbar]$.

To describe the *outgoing* resonance of the Γ_3^- phonon scattering process, the order of the transition matrix elements in Eq. (3.1) has to be reversed, resulting in the same time dependence as for the incoming resonance.

In contrast to one-phonon scattering, the two-phonon process [compare Fig. 1(c)] allows to create excitons with different kinetic energies and wave vectors because of the phonon participation in the absorption and emission part of the Raman process. As is well known from Raman studies under stationary excitation,[21] the two-phonon process becomes resonant for laser photon energies (E_L) larger than the indirect absorption threshold $E_Q + \hbar\Omega(\Gamma_3^-)$ whereby the kinetic energy of the exciton states is given by $\epsilon = E_L - E_Q - \hbar\Omega(\Gamma_3^-)$. The time-dependent intensity of the $2\Gamma_3^-$ process is obtained from Eq. (3.1) by replacing $\mathbf{M}_m^{\mathrm{EQ}}$ by $\mathbf{M}_{l,m}^{\mathrm{ED}}$ and summing twice over the phonon modes.

Figure 2 displays two scattering spectra showing the processes described above. In the right-hand side, excitation is accomplished at E_L=2.048 eV, i.e., slightly above the Γ_3^- phonon assisted exciton absorption edge. Besides the strong Γ_3^- and much weaker Γ_5^- one-phonon replica ($X^0-\Gamma_3^-$; $X^0-\Gamma_5^-$), two-phonon scattering occurs in this situation, too, giving rise to the line $2\Gamma_3^-$. The luminescence line X^0 is due to the orthoexciton (zero-phonon) recombination. Its remarkably narrow width compared to the laser line is a clear indication of the polariton character of the exciton. Following excitation and relaxation, the emission originates from the bottleneck region of the polariton dispersion curve where the homogeneous linewidth is minimal.[26] For excitation in resonance with

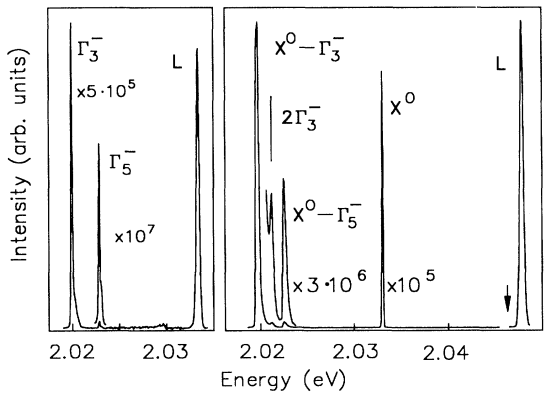

FIG. 2. Light-scattering spectra of Cu_2O at T=1.8 K. Right-hand side: excitation (L) at E_L=2.048 eV, i.e., ϵ = 1.5 meV above the Γ_3^- phonon-assisted absorption edge marked by the arrow. X^0: resonance fluorescence of the $1S$ orthoexciton at energy E_Q = 2.0329 eV. The lines $X^0 - \Gamma_3^-$ and $X^0 - \Gamma_5^-$ at lower energies are corresponding phonon replicas. $2\Gamma_3^-$ marks the resonantly enhanced two-phonon scattering involving Γ_3^- phonons. Left-hand side: excitation (L) at the quadrupole resonance of the $1S$ orthoexciton; the one-phonon scattering processes are denoted by Γ_3^- and Γ_5^-. Wave vectors and polarizations of the incident and scattered light: $\mathbf{k}_L$,$\mathbf{k}_S$ || [001]; $\mathbf{e}_L$, $\mathbf{e}_S$ || [100].

the orthoexciton state at $E_L = E_Q = 2.0329$ eV (left-hand side) only one-phonon scattering is visible.

B. Magnetic-field splitting of the Γ_5^+ exciton

For quantum beats to be created from the $1S$ orthoexciton, an external magnetic field $\mathbf{B}$ was applied. In the presence of this field, the Γ_5^+ states split into three components (see below inset of Fig. 3) whereby the energy and wave functions of the excitons are described by the effective Zeeman Hamiltonian[27]

$$H_z = \tfrac{1}{2}(g_c + g_v)\mu_B \mathbf{F}\cdot\mathbf{B}, \tag{3.2}$$

where $\mathbf{F}$ is a pseudospin vector with z-component $F_z = \pm 1, 0$, the quantities g_c and g_v are the g values for conduction and valence bands, and μ_B is the Bohr magneton. In our experiments we applied the magnetic field parallel to the incident and scattered light ($\mathbf{B} \parallel \mathbf{k}_L \parallel \mathbf{k}_S$), i.e., in Faraday geometry. In this case only the $F_z = \pm 1$ states are optically allowed interacting with light of circular ($\sigma^{\pm}$) polarizations. These states show a linear Zeeman energy splitting

$$\Delta E = |g_c + g_v|\mu_B B \tag{3.3}$$

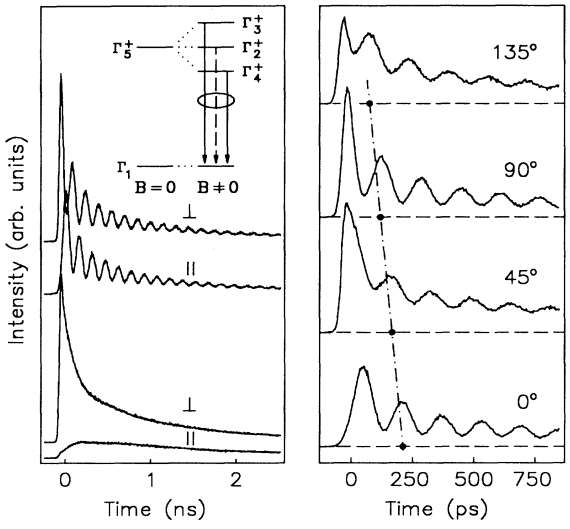

FIG. 3. Left: Time-dependent polarized intensity of the $1\Gamma_3^-$ phonon scattering process at zero magnetic field (lower curves) and for B=0.25 T (upper curves) excited at the quadrupole exciton ($E_L = E_Q$). The exciting light with $\mathbf{k}_L \parallel$ [001] is polarized along $\mathbf{e}_L \parallel$ [100], the scattered light along $\mathbf{e}_S \parallel$ [100] ($\parallel$) and [010] ($\perp$). Inset: Energy-level scheme and magnetic-field splitting of the $1S$ orthoexciton. Beating occurs between the optically allowed Γ_3^+ and Γ_4^+ states. Right: Quantum beats at B=0.25 T for different detection polarizations to demonstrate the selection rules in Table I. Corresponding beat maxima are marked to make clear the systematic phase shifts of subsequent signals.

so that the coherent excitation of these states by short, linearly polarized laser pulses should give rise to beating in the Raman signal with a corresponding oscillation frequency $\omega = \Delta E/\hbar$.

To calculate the scattered intensities in the case of an applied magnetic field $\mathbf{B}$, the mixing of the exciton states must be considered. To this end, the exciton is described by a set of unperturbed wave functions $\phi_{yz}, \phi_{zx}, \phi_{xy}$ transforming as yz, zx, and xy, respectively. With the magnetic field applied, each level can be described by a linear combination of these functions[24] according to

$$\Phi_m = \alpha_m \phi_{yz} + \beta_m \phi_{zx} + \gamma_m \phi_{xy}, \tag{3.4}$$

where the values of the coupling parameters α_m, β_m, and γ_m depend on the directions of the magnetic field and the wave vector and polarization of the light field.

In Table I, the intensities are listed that were calculated from Eq. (3.1) for the chosen Faraday geometry and different polarizations taking into account the mixing of the exciton states [Eq. (3.4)]. For linearly polarized excitation along [001], the beat signal for parallel (0°) and perpendicular (90°) polarizations shows complete modulation (degree of modulation = 1), while for polarizations under 45° and 135° ($\mathbf{e}_S \parallel$ [110] and [$\bar{1}$10], respectively) the degree of modulation is only 1/2. Contrary to these cases, circularly polarized detection ($\sigma^{\pm}$), due to the selection rules, probes just one of the exciton states so that they are no longer indistinguishable and no beating occurs. Moreover, Table I shows that the oscillations for polarizations orthogonal to each other are phase shifted by a factor of π. This is of advantage for extracting the coherent part from the scattered intensities by a simple subtraction.

TABLE I. Calculated time-dependent $1\Gamma_3^-$ phonon Raman line intensities. The wave vectors of the incident and scattered light and the magnetic field are $\mathbf{k}_L \parallel \mathbf{k}_S \mathbf{B} \parallel$ [001]. The corresponding light polarizations ($\mathbf{e}_L, \mathbf{e}_S$) are as shown. For reasons of clearness we assumed $T_2' = 0$, i.e., $\tau_{\rm coh} = 2T_1$. A factor $\exp(-2t/\tau_{\rm coh})$ is omitted in all intensity expressions (from Ref. 35).

$\mathbf{e}_L$	$\mathbf{e}_S$	$I(\mathbf{e}_L, \mathbf{e}_S, t)$ with $\mathbf{B} \neq 0$
[100]	[100] (0°)	$I_0(1 - \cos\omega t)$
	[010] (90°)	$I_0(1 + \cos\omega t)$
	[110] (45°)	$I_0(1 + 1/2 \sin\omega t)$
	[$\bar{1}$10] (135°)	$I_0(1 - 1/2 \sin\omega t)$
	[1 i 0] (σ^+)	I_0
	[1 $\bar{\rm i}$ 0] (σ^-)	I_0
[110]	[110] (0°)	$I_0(1 - 1/2 \cos\omega t)$
	[$\bar{1}$10] (90°)	$I_0(1 + 1/2 \cos\omega t)$

C. Exciton-polariton relaxation

So far the discussion was restricted to the exciton state with the exciton-photon interaction neglected. Coupling between the exciton and the light field, however, leads to the formation of polaritons accompanied by a splitting of the uncoupled photon-exciton dispersion curves near their crossing point in two branches (see e.g., Ref. 28). Because of the quadrupole character of the exciton transition the splitting is small (of the order of 20 μeV) but associated with a very strong dispersion of the polariton branches within a narrow range of wave vector $\mathbf{K}$ (for a quantitative computation of the dispersion curves in Cu_2O see Refs. 19 and 20). Consequently, polaritons created at the entrance surface of the sample having only slightly different energies around the exciton resonance propagate with group velocities $v_g(\mathbf{K})$ that are strongly dispersive and vary by orders of magnitude.

The consideration of the polariton character has a dramatic effect on the relaxation times. This is because, besides intrinsic processes due to elastic and inelastic scattering, the transformation of polaritons at the rear of the crystal into external photons represents an additional decay channel. Neglecting the traveling time of photon states at the scattered photon energy E_S (which for typical sample dimensions is of the order of 5 ps, i.e., smaller than all relevant relaxation times), this decay is characterized by the time-of-flight rate

$$\Gamma_{\rm tf}(\mathbf{K}) = \frac{v_g(\mathbf{K})}{d} \tag{3.5}$$

with d denoting the sample length along the polariton flight direction (see also Ref. 29). This rate may also be interpreted as the probability of the polaritons to escape from the sample and, as will be shown below, determines the time-dependent scattering intensity at small times.

Accordingly, the total exciton-polariton relaxation rate (with $\delta E_{\rm hom} = \hbar\Gamma_{\rm tot}$) may be written as

$$\Gamma_{\rm tot} = \Gamma_{\rm ex} + \Gamma_{\rm tf}(\mathbf{K}) + \Gamma_{\rm elast} \, . \tag{3.6}$$

Here $\Gamma_{\rm ex} = 1/T_1$ represents the inelastic scattering rate due to the exciton part of the polariton. In Cu_2O, it essentially consists of three contributions[30]

$$\Gamma_{\rm ex} = \Gamma_{\rm ac} + \Gamma_{o-p} + \Gamma_d, \tag{3.7}$$

where the most important term $\Gamma_{\rm ac}$ accounts for intraband scattering of excitons by phonons,[21] Γ_{o-p} represents the conversion rate of orthoexcitons into paraexcitons[31] and Γ_d characterizes defect-induced exciton decay.[32] The last term in Eq. (3.6) describes elastic scattering processes of polaritons into different momentum states and between the degenerate exciton states ($F_z = 0, \pm 1$). These elastic processes just give rise to the hot polariton luminescence but are expected to be strongly sample dependent.

In Cu_2O at low temperatures, exciton-phonon scattering arises entirely from interaction with longitudinal acoustic (LA) phonons and for which the temperature dependence may be calculated theoretically.[26] In this case the transition rate from an initial exciton state $|1S(\mathbf{K}_i)\rangle$ with kinetic energy $\epsilon_i = \hbar^2 k_i^2/2M^*$ to a final state $|1S(\mathbf{K}_f)\rangle$ with $\epsilon_f = \hbar^2 k_f^2/2M^*$ is given by[33]

$$\Gamma_{\rm ac}^{S,\rm AS}(\epsilon_i, \epsilon_f, T) = C_{\rm ac} \frac{(\epsilon_i - \epsilon_f)^2}{\sqrt{\epsilon_i/\epsilon_0^*}} \times \left[n_{\rm phon}(|\epsilon_i - \epsilon_f|, T) + \tfrac{1}{2} \pm \tfrac{1}{2} \right], \tag{3.8}$$

with the abbreviations

$$C_{\rm ac} = \frac{1}{4\pi} \frac{E_D^2}{\hbar^4 \rho u_L^5}, \tag{3.9}$$

$$\epsilon_0^* = \frac{1}{2} M^* u_L^2, \tag{3.10}$$

and the $\pm$ signs for Stokes (S) and anti-Stokes (AS) scattering. E_D and u_L are the deformation potential and sound velocity of the LA phonons, M^* is the effective exciton mass, and ρ the mass density of Cu_2O.

The final exciton energy ϵ_f is determined by momentum and energy conservation. For S scattering it varies according to

$$\max\left\{ \epsilon_i, \epsilon_i - 4\epsilon_0^* \left(\sqrt{\epsilon_i/\epsilon_0^*} - 1 \right) \right\} \le \epsilon_f \le \epsilon_i \, , \tag{3.11}$$

and for AS scattering according to

$$\min\left\{ \epsilon_i, \epsilon_i - 4\epsilon_0^* \left(1 - \sqrt{\epsilon_i/\epsilon_0^*} \right) \right\} \le \epsilon_f \le \epsilon_i + 4\epsilon_0^* \left(1 + \sqrt{\epsilon_i/\epsilon_0^*} \right) \, . \tag{3.12}$$

The phonon occupation number for a lattice temperature T is given by the Bose-Einstein distribution

$$n_{\rm phon}(|\epsilon_i - \epsilon_f|, T) = \frac{1}{\exp(|\epsilon_i - \epsilon_f|/k_B T) - 1} \, , \tag{3.13}$$

with the Boltzmann constant k_B. To calculate the total scattering rate $\Gamma_{\rm ac}$ one has to integrate over all possible energies of the final states and add up the S and AS contributions

$$\Gamma_{\rm ac} = \int_A^B \Gamma_{\rm ac}^S(\epsilon_i, \epsilon_f, T) d\epsilon_f + \int_C^D \Gamma_{\rm ac}^{\rm AS}(\epsilon_i, \epsilon_f, T) d\epsilon_f \, , \tag{3.14}$$

whereby the integration limits are taken from Eqs. (3.11) and (3.12), respectively.

Calculations of the exciton-phonon scattering rate using Eq. (3.14) show that in the measured low-temperature range Γ_{o-p} and Γ_d are much smaller compared to $\Gamma_{\rm ac}$ (see Sec. IV D) which itself is found to be $\mathbf{K}$ independent. The conversion of orthoexcitons into paraexcitons takes place by interaction with one acoustic and one optical phonon[31] with rates of the order of $\Gamma_{o-p} \approx 2.5 \times 10^8 \ {\rm s}^{-1}$ at 2.5 K.[34] Γ_d is essentially caused by nonradiative recombination being in the first place relevant for the paraexciton lifetime. According to the inves-

tigations of Mysyrowicz *et al.*,[32] the paraexciton lifetime is determined by the sample quality, i.e., by extrinsic effects. Their measurement in a laboratory grown crystal and in a high quality natural crystal yielded lifetimes of 10 ns and 13 μs, respectively, corresponding to defect-induced rates of about 10^8 and 10^5 s^{-1}. For these reasons $\Gamma_{o\text{-}p}$ and Γ_d can be neglected.

As the polariton near the crossing point is considered a mixed state between exciton and photon having equal weights, the acoustic phonon scattering rate into a final purely excitonic state is given by $\Gamma_{ac}/2$ (see Sec. IV D).[28,35]

IV. EXPERIMENTAL RESULTS AND ANALYSIS

A. $1\Gamma_3^-$ phonon scattering processes

Using the geometry described in Sec. II we have investigated quantum beating both for the $1\Gamma_3^-$ and $2\Gamma_3^-$ phonon process (see Fig. 2). In Fig. 3 (left-hand side), the time dependence of the polarized one-phonon scattering intensity is shown excited precisely at the quadrupole exciton ($E_L = E_Q$) with $\mathbf{e}_L \parallel [100]$ and analyzed with $\mathbf{e}_S \parallel [100]$ and $\parallel [010]$ ($\parallel$ and $\perp$, respectively). As displayed in the lower two curves for B=0 T, except for a small depolarized hot-luminescence component complete polarization occurs as expected from the selection rules that predict an intensity ratio $I_\perp : I_\parallel = 1 : 0$ (see Table I for ω =0). The intensity occurring in the forbidden ($\parallel$) polarization represents the hot luminescence from the exciton states. It is rather weak indicating a small contribution of the pure dephasing processes to the homogeneous linewidth [Eq. (1.1)].

It is worth noting at this point that without a magnetic field no beating occurs in the one-phonon scattering in spite of the inherent polariton splitting described above. The reason is that in the one-phonon process considered here, the polariton states excited at the two branches interact with two different phonons. The scattering processes, therefore, do not end in the same final state but rather correspond to distinguishable relaxation channels that cannot engender beating.[1] This situation is quite different from recent pulse transmission experiments in Cu_2O (Refs. 19 and 20) in which simultaneous excitation of states of the upper and the lower polariton branches by a spectrally broad laser pulse led to an oscillatory structure in the transmitted pulse intensity. As phonons are not involved, this process corresponds to resonance scattering leading back into a common final state which is the crystal ground state. This makes the two channels of polariton decay indistinguishable and results in a beating structure.

With a magnetic field applied (B=0.25 T; upper two curves in Fig. 3) and the exciton states split, the coherent nature of the scattering process is revealed by the occurrence of quantum beats. They are observed for both polarizations and are superimposed on a small incoherent luminescence background. According to the selection rules in Table I, the oscillations are phase shifted by a factor of π. Their slowly decreasing amplitudes imply relatively long coherence times and show that the dephasing mainly arises from the depopulation of the involved exciton-polariton states. As had been decribed previously,[8] the analysis of these signals was accomplished by performing a discrete Fourier transformation of the coherent intensity contribution ($I_\perp - I_\parallel$). Fitting a Lorentzian to the transformed data, from the position (ν) and width ($\Delta\nu$) of the obtained spectral peak an energy splitting $h\nu = \Delta E \approx 26$ μeV (6.3 GHz) and a coherence time $\tau_{coh} = 2/\pi\Delta\nu \approx 1$ ns were deduced. This corresponds to a homogeneous linewidth of only $\delta E_{hom} = 1.4$ μeV. For very long times the beats become entirely damped out, the intensity ratio $I_\perp : I_\parallel = 1$ indicating unpolarized scattering. This demonstrates the anticipated transformation from coherent Raman scattering to incoherent hot luminescence. Furthermore, the hot-luminescence background is found to be almost field independent. This is in full agreement with the theoretical expectations that the quantum beats show up only in the polarized Raman part of the scattered intensity sitting on top of the hot luminescence component.

Measurements to test the calculated intensities by using different detection polarizations are presented in Fig. 3 (right-hand side). Closer inspection of the oscillatory structure and comparison with Table I gives excellent agreement with regard to the degree of modulation and the phase shift. In particular the figure makes clear the $\pi/2$ phase shift found between the corresponding beat maxima by rotating the analyzer in steps of 45° which is entirely consistent with the calculated intensity expressions (for an interpretation of this phase shift in terms of the Hanle effect, see Ref. 12).

The oscillation frequency of the beat signal can be used to explore the Zeeman splitting of the Γ_5^+ exciton state as function of the magnetic field (see Fig. 4). From analyzing measurements up to 1 T we found a strictly linear dependence for the optically allowed $M = \pm 1$ components. Using Eq. (3.3) to fit the data gives an accurate effective g value of $|g_c + g_v| = 1.78 \pm 0.05$ which is

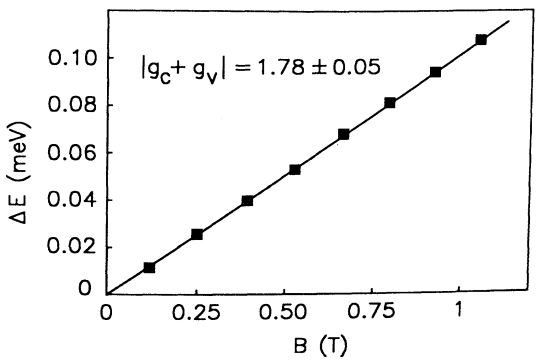

FIG. 4. Zeeman splitting of the Γ_3^+ and Γ_4^+ ($M = \pm 1$) exciton sublevels derived from the oscillation frequency as function of magnetic-field strength. Scattering geometry as in Fig. 3. The experimental data are shown with a fit (full line) according to Eq. (3.3).

slightly larger than that reported earlier from high-field measurements.[27] We especially emphasize that even at the highest field of 1 T no spectral splitting of the exciton quadrupole emission (line X^0 in Fig. 2) could be detected. This is because of inhomogeneous line broadening and demonstrates very clearly the enormous potential of quantum beating to reveal small energy splitting of states.

In addition to the Zeeman quantum beats, we have observed beating due to zero-field splittings that are found strongly dependent on the investigated spot at the sample.[35] In Fig. 5 (left) the time dependence of the polarized one-phonon intensity is shown for different linear excitation polarizations. Although here no magnetic field was applied, a clear beating structure is observed and ascribed to exciton splitting caused by an internal local strain. The experimental finding resembles that in the recently studied case of CdS.[8] For the ±45° polarizations ($\mathbf{e}_L \parallel [110]$ and $[\bar{1}10]$) only one of the linearly polarized states is excited so that the quantum-beats vanish. For all other excitation polarizations a weakly modulated quantum-beat signal is observed. The degree of modulation is very small, due to the fact that only a small number of the states in the investigated region of the sample are subject to strain splitting. All others contribute to the polarized intensity for which, in this case, the selection rules predict a ratio $I_\perp : I_\parallel = 3 : 1$ (see Ref. 35 and also Table I). The corresponding Fourier spectra are displayed in the right-hand side of Fig. 5. From these an energy splitting of $\Delta E \approx 8$ μeV (about 2 GHz) and coherence times between 0.8 and 1.1 ns were deduced in spite of the poor signal-to-noise ratio.

According to the theory developed in Sec. III A [Eq. (3.1)], one-phonon scattering in the incoming and outgoing resonance case [cf. Figs. 1(a) and 1(b)] can be expected to give identical beat signals. This is indeed the case as seen by comparing the corresponding experimental data in Fig. 6. The analysis of the signals, apart from an energy splitting of 26 μeV at B=0.25 T, gives a coherence time of $\tau_{coh} \approx 1$ ns identical for the two excitation conditions. This justifies the assumptions of the theory and implies that the phonon itself does not destroy the phase of the intermediate states. The participation of phonons obviously is necessary only for reasons of energy and momentum conservation but has no influence at all on the exciton coherence.

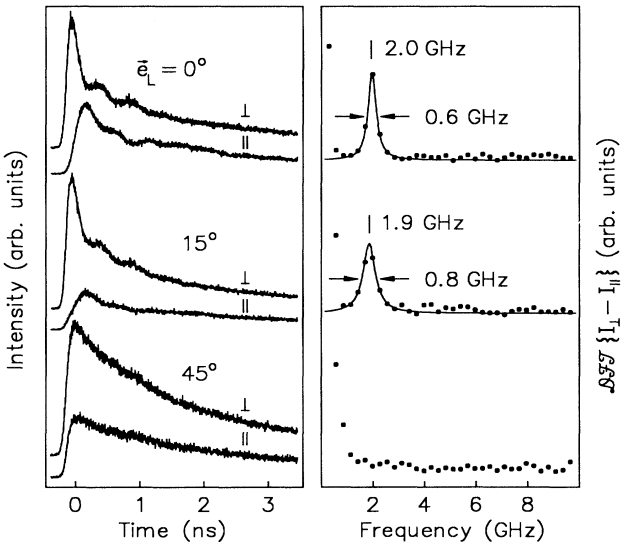

FIG. 5. Quantum beating due to a zero-field strain splitting of the exciton. Left: Time-dependent polarized $1\Gamma_3^-$ phonon intensity for different excitation polarizations. 0° and 45° are equivalent to $\mathbf{e}_L \parallel [100]$ and [110], respectively. Right: Fourier transforms of corresponding difference intensities $I_\perp - I_\parallel$ (full points) together with a fit to a Lorentzian (full curves) using the parameters given in the figure.

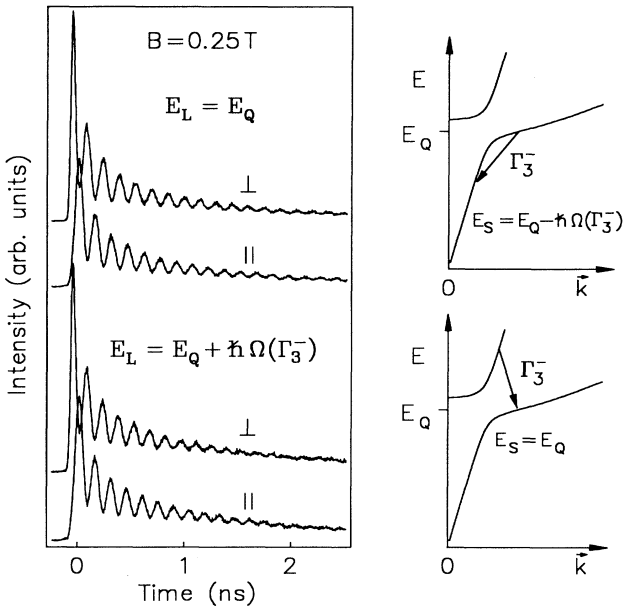

FIG. 6. Left: Time dependence of the polarized intensity of the $1\Gamma_3^-$ phonon scattering process at B=0.25 T in the case of the incoming (upper part) and outgoing resonance with the quadrupole exciton (lower part). The excitation and detection conditions are as in Fig. 3. Right: schematic representation of the corresponding phonon scattering processes (arrows) and polariton dispersion.

B. $2\Gamma_3^-$ phonon scattering

To study the exciton relaxation behavior at higher energies, experiments were performed with the $2\Gamma_3^-$ phonon line that gradually emerges when the excitation is tuned into the exciton band [see Figs. 1(c) and 2]. In Fig.7 a typical result for an exciton kinetic energy of $\epsilon = E_L - [E_Q + \hbar\Omega(\Gamma_3^-)] \approx 0.2$ meV at B=0.25 T is presented. Compared with one-phonon scattering, much larger contributions from incoherent processes are found with only a small oscillating structure sitting on top. To a large part the background is due to the emission from thermalized exciton states populated via the nonresonant $1\Gamma_3^-$ phonon-assisted absorption process that simultaneously takes place.

The evaluation of the $2\Gamma_3^-$ phonon scattering signals by means of Fourier analysis shows that the coherence time is drastically reduced with increasing exciton kinetic energy. At the lowest energy close to the bottom of the

exciton band ($\epsilon \approx 0$ meV) we find $\tau_{coh} = 820$ ps, practically identical with the value derived from one-phonon scattering, while for $\epsilon \approx 0.2$ meV it has already dropped to $\tau_{coh} = 510$ ps. To get comparable data in spite of the observed local dependence, special precautions were taken to guarantee that the measurements were done exactly at the same sample position. For higher kinetic energies ($\epsilon > 0.3$ meV), the quantum-beat signals completely vanish because of the rapidly increasing importance of relaxation processes. As anticipated, the energy splittings obtained as a function of the magnetic field from one- and two-phonon scattering are the same.

C. Influence of polariton propagation

As pointed out above (Sec. III C), the polariton nature of the exciton, via the strongly dispersive time-of-flight damping $\Gamma_{tf}(\mathbf{K})$ [cf. Eq. (3.5)], has a drastic effect on the coherently scattered one-phonon intensity $I_\perp - I_\parallel$. In Fig. 8 (left), the measured time dependence is represented for two different bandwidths ΔE_L of the excitation pulse. The upper curve was obtained for excitation with a spectrally broad pulse and represents the difference of the polarized signals for $B = 0$ T in Fig. 4. Polaritons are impulsively excited with a wide spread in group velocity and, hence, arrive at quite different times at the rear of the sample. A large portion is traveling fast resulting in the rapid initial decay of intensity, while the rest is much slower arriving only at later times. In contrast, the lower curve in Fig. 8 was measured for narrow spectral width excitation. In that case all polaritons have nearly uniform group velocity. They arrive almost simultaneously, the exponential decay reflecting essentially their coherence time.

To account for this polariton effect, Eq. (A7) has to be modified by replacing E_m by the polariton dispersion $E_m(\mathbf{K}_j)$ (j = UP, LP for the upper and lower branch) and by setting $\delta E_{hom} = \hbar\Gamma_{tot}$ [Eq. (3.6)], respectively, so that the scattering amplitude $\Psi_m(t)$ becomes wave-vector dependent.[11] Rewriting then Eq. (A6) to include the polariton effect, one obtains for the time-dependent polarized $1\Gamma_3^-$ phonon signal

$$I^{CS}(t, \mathbf{e}_L, \mathbf{e}_S) \propto \sum_{\mathbf{K}_j} \sum_{l=1,2} \left| \sum_m (\mathbf{M}_m^{EQ} \cdot \mathbf{e}_L)(\mathbf{M}_{l,m}^{ED} \cdot \mathbf{e}_S)^* \Psi_{m,\mathbf{K}_j}(t) \right|^2 . \quad (4.1)$$

Corresponding to the spectral width of the laser pulse, the contributions with different wave vectors of the upper and lower polariton branch have to be added up as implied by the outer (incoherent) summation over $\mathbf{K}_j$. The right-hand side of Fig. 8 displays the scattered intensities numerically calculated from Eq. (4.1) for the indicated spectral bandwidths. Very close to our experimental conditions, the exciting laser pulse was approximated by a single-sided exponential

$$F_L(t) = \sqrt{\Delta E_L/\hbar}\,\Theta(t) \exp(-\Delta E_L t/(2\hbar)) \quad (4.2)$$

with spectral widths ΔE_L as indicated. Instead of the actual grating monochromator which is difficult to treat theoretically, for the calculation a Fabry-Perot was assumed as spectral filter having an amplidute transmission function

$$F_S(t) = \sqrt{\Delta E_S/\hbar}\,\Theta(t) \exp(-\Delta E_S t/(2\hbar)) \quad (4.3)$$

with the spectral bandwidth set to $\Delta E_S = 0.25$ meV. In the calculation, we used the oscillator strength (entering the polariton dispersion and, hence, the time-of-flight broadening) known from pulse propagation experiments with the same samples ($f_0 = 3.6 \times 10^{-9}$).[19,20] The only other parameter to be specified is the sum of the inelastic and elastic relaxation rates $\Gamma_0 = \Gamma_{ex} + \Gamma_{elast}$ in Eq. (3.6). Obviously, this rate is identical with the oscillator damping used in classsical polariton theory,[36] and, due to the small range of polariton wave vectors involved, can be taken as constant. Using the damping constant derived from the propagation experiments ($\Gamma_0 = 1.0 \times 10^9$ s^{-1}),[19] very good agreement is achieved with the experimental results. Comparing with the coherence time derived from the quantum-beat experiments

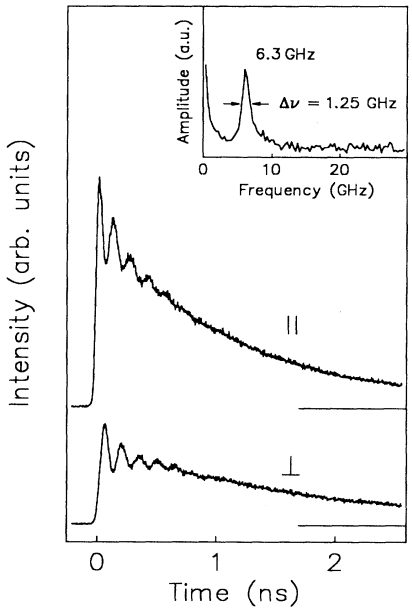

FIG. 7. Time dependence of the polarized intensity of the $2\Gamma_3^-$ phonon scattering process for B=0.25 T. Excitation at $E_L = 2.0467$ eV slightly above the $1S$ exciton absorption ($\epsilon \approx 0.2$ meV). The other conditions are as in Fig. 3. Inset: Fourier transform calculated from ($I_\perp - I_\parallel$). The peak width corresponds to $\tau_{coh} = 510$ ps.

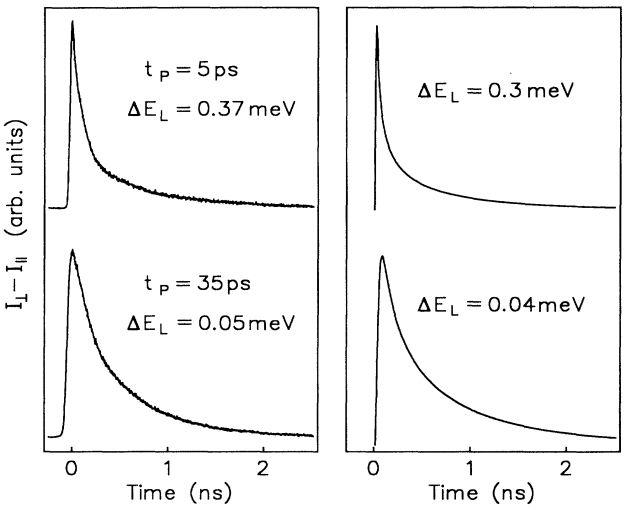

FIG. 8. Time dependence of the $1\Gamma_3^-$ phonon Raman contribution excited with two different laser pulses (B=0 T). ΔE_L and Δt_P are the spectral and temporal widths of the pulses. Left: experimental curve. Right: calculation according to Eq. (4.1) as discussed in the text.

described above ($\tau_{coh} \simeq 1$ ns), we can draw the conclusion that the contribution of the time-of-flight rate to the total relaxation rate is of the same order as those of all other relaxation processes. This unambiguously proves the necessity to include polariton effects in a quantitative analysis of light scattering from direct exciton states.

D. Temperature dependence of the $1\Gamma_3^-$ process

The decay of the quantum-beat signal allows one to follow the dependence of the coherence time of the exciton on external parameters like impurity content and others. As an example, Fig. 9 shows the Raman signal ($I_\perp - I_\parallel$) at three different temperatures. From the number of oscillations that develop it is right away obvious that the coherence time rapidly decreases by raising the temperature only slightly from 2.1 K to 10 K. The corresponding rate is plotted in the inset, its temperature dependence being ascribed to inelastic scattering.

Recalling that LA phonon scattering is the dominant energy relaxation mechanism, we may rewrite Eq. (1.1) in the form

$$\frac{1}{\tau_{coh}}(T) = \frac{1}{4}\Gamma_{ac}(T) + \frac{1}{2}\langle\Gamma_{tf}\rangle + \frac{1}{T_2'}\,, \qquad (4.4)$$

whereby we account for the polariton nature of the exciton[26,35] by the additional factor 1/2 in front of Γ_{ac} and by an average time-of-flight rate $\langle\Gamma_{tf}\rangle$ (cf. Sec. III C). Also we assume pure dephasing with rate $1/T_2'$ temperature independent.

To fit the experimental data in Fig. 9 by Eq. (4.4), the pure dephasing rate was determined with the help of Eq. (1.1) and the measured low-temperature (2.1 K) values $\tau_{coh} = 800$ ps and $T_1 = 1/[\Gamma_{ac}(T)/2 + \langle\Gamma_{tf}\rangle] = 910$ ps for this sample giving $1/T_2' = 0.7$ GHz. The average time-of-flight rate under the given excitation conditions is about 1×10^9 s^{-1}. $\Gamma_{ac}(T)$ then was calculated from Eqs. (3.8) to (3.14) using the deformation potential for LA phonons ($E_D = 2.1$ eV) (Ref. 37) and the mass density of Cu_2O ($\rho = 6.1 \times 10^3$ kg m^{-3}).[38] According to experiment, the kinetic energy of the exciton was chosen $\epsilon = 0.01$ meV.

As seen from the inset of Fig. 9, excellent agreement is achieved between the experimental data and the calculation with no adjustable parameters. It confirms the suggestion that at increasing temperatures the major dephasing mechanism of the polaritons is inelastic scattering by LA phonons. As exciton-phonon scattering due to the small number of available final states is strongly reduced at the lowest temperatures, this explains the relatively long coherence times found in Cu_2O. Also our samples are of high structural quality so that scattering from static imperfections is negligible.

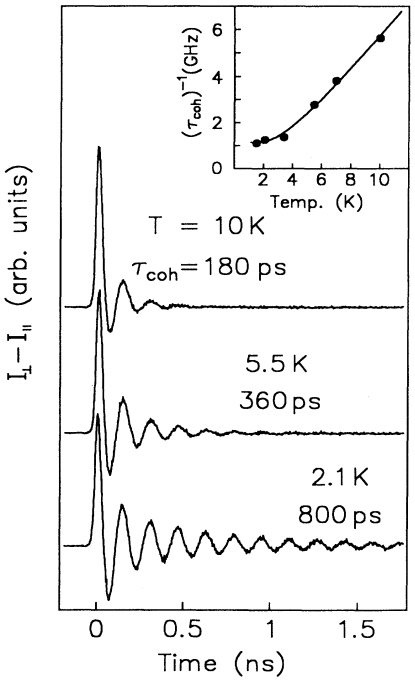

FIG. 9. Quantum beats in the $1\Gamma_3^-$ phonon line at different temperatures (B=0.25 T). Excitation and detection conditions are as in Fig. 3. Inset: measured (points) and calculated (line) temperature dependence of the coherence decay rate of the Γ_5^+ exciton polariton (see text).

V. CONCLUDING REMARKS

With the investigations in Cu_2O we have demonstrated that quantum-beat spectroscopy in resonance light scattering is an important and elegant method to study excitons in semiconductors. Not only that, but the beat frequencies as a function of magnetic field provide extremely small energy splittings and precise g values. Also the detailed analysis of the temporal characteristics of the beating, especially at different temperatures, gives quantitative information on the dephasing and relevant scattering mechanisms. Moreover, the particular direct (quadrupole) exciton offers the opportunity to reveal and clarify the influence of the polariton nature and phonon interaction on the intermediate state coherence. Finally, the method allows a clear distinction of Raman scattering and hot luminescence solving a question that for the $1S$ yellow exciton in Cu_2O had led to much controversy in the literature.

ACKNOWLEDGMENTS

The authors appreciate the cooperation with D. Fröhlich, A. Kulik, and B. Uebbing of the University of Dortmund, who also provided the Cu_2O samples. They gratefully acknowledge support by the Deutsche Forschungsgemeinschaft.

APPENDIX

In this appendix we present a brief derivation of the theory of time-resolved light scattering leading to Eqs. (3.1) and (4.1) and allowing one to discuss the relevant physical parameters that determine Raman and hot-luminescence processes.

As is well known, a physically meaningful time-resolved spectrum of light can only be defined by the use of a measuring setup (see e.g., Ref. 18) that here we assume to consist of a spectral filter [with transmission function $F_S(t)$] to select the frequency of the light field and of a time-resolving detector to measure its temporal behavior. This gives the following expression for the experimentally registered counting rate[18]:

$$R(\omega_S,t)=\int_{-\infty}^{\infty}dt'\int_{-\infty}^{\infty}dt''F_S^*(t-t')F_S(t-t'')\times\langle\, E_S^{(-)}(t')\,E_S^{(+)}(t'')\,\rangle\,. \tag{A1}$$

The expression in brackets is the quantum mechanical field correlation function with $E_S^{(+)}(t)$ denoting the positive frequency part of the electric field operator of the light field under investigation. The maximum amount of information on the light field can be obtained, if the spectral filter is *bandwidth limited*, i.e, its spectral and temporal transmission functions are Fourier transforms of each other (for examples see Refs. 11 and 18).

To calculate the field correlation function, we apply standard perturbation theory using Feynman diagrams to systematically take all contributions to the light scattering of an exciton system interacting with a thermal phonon bath into account.[39,18] Inserting the usual mode expansion of the field operator into the field correlation function we obtain the following expression:[18]

$$\langle\, E_S^{(-)}(t')\,E_S^{(+)}(t'')\,\rangle=\langle\mathbf{k}_S\mathbf{e}_S|\mathrm{Tr}_B[U(t',t_0)\times\rho(t_0)U(t'',t_0)^\dagger]|\mathbf{k}_S\mathbf{e}_S\rangle. \tag{A2}$$

Here due to the spectral and spatial selection of the optical filter only modes with a certain wave vector $\mathbf{k}_S$ and polarization $\mathbf{e}_S$ are observed. The trace operation is to be performed over the bath states. $U(t,t_0)$ is the time-development operator and $\rho(t_0)$ is the density matrix of the system at time t_0, which for $t_0\to-\infty$ is assumed to be

$$\rho(-\infty)=|\mathbf{k}_L\mathbf{e}_L\rangle\langle\mathbf{k}_L\mathbf{e}_L|\otimes\rho_B. \tag{A3}$$

Here ρ_B denotes the density matrix of the bath in thermal equilibrium. The exciting laser pulse (wave vector $\mathbf{k}_L$, frequency ω_L, and polarization $\mathbf{e}_L$) is specified by a photon state $|\mathbf{k}_L\mathbf{e}_L\rangle$ that corresponds to an envelope function $F_L(t)$ of the laser pulse.

In the case of weak interaction between exciton and bath states, only laddertype diagrams[39] contribute significantly to the scattered intensity. Furthermore, to simplify the calculations, we assume the following.

(1) The memory time of the bath is short compared with the time scales of the exciton and photon system (Markoff approximation).

(2) The exciton propagator contains all relaxation processes of the exciton states (denoted by quantum numbers α) as a complex self-energy with homogeneous linewidth $\delta E_{\mathrm{hom},\alpha}=\hbar/2\tau_{\mathrm{coh},\alpha}$, where $\tau_{\mathrm{coh},\alpha}$ is the total coherent lifetime, which in this case is identical to the optical dephasing time T_2. In the Markoff approximation,[39] $\delta E_{\mathrm{hom},\alpha}$ can be decomposed into the contributions due to energy-relaxation $1/T_{1,\alpha}$, containing the radiative decay, and the pure dephasing by elastic interactions w_α

$$w_\alpha=\sum_{\alpha'}\overline{h}_{\alpha,\alpha'}\,, \tag{A4}$$

with $\overline{h}_{\alpha,\alpha'}$ denoting the squared average exciton-bath interaction matrix element

$$\overline{h}_{\alpha,\alpha'}=2\pi\sum_{l,l'}|h_{\alpha,\alpha'}(l,l')|^2n_{l'}(n_l+1)\delta(\epsilon_l-\epsilon_{l'}). \tag{A5}$$

Here the bilinear interaction matrix elements $h_{\alpha,\alpha'}(l,l')$ describe elastic scattering between bath states l,l' and exciton states α,α'. n_l denotes the phonon occupation number. This results in relation (1.1) with $T'_{2,\alpha}=2/w_\alpha$.

(3) The exciton-photon coupling is expressed by $\mathbf{M}_\alpha\cdot\mathbf{e}_{L,S}$ with appropriate transition moments $\mathbf{M}_\alpha$ that in case of scattering by phonons also include the exciton-phonon interaction. Accordingly, the Raman phonons correspond to outer lines in the Feynman diagrams.[15] Therefore, the summations in Eq. (A6) involve only exciton states at the same wave vector, the final result being

obtained by summing the scattered intensities of all participating states with different $\mathbf{k}$. The phonon dynamics thus should have no influence on the coherence properties of the intermediate exciton states.

The lowest order diagram (zero order in the exciton-bath interaction) describes processes that proceed without loss of coherence of the exciton states and will be interpreted, therefore, as *coherent scattering* (CS). It represents the true Raman part of the spectrum. On the other hand, all diagrams with one or more exciton-bath interaction vertices represent processes during which the phase memory is lost (instantaneously in the Markoff approximation) and, therefore, correspond to *hot luminescence* (HL).

The coherent contribution to the scattering spectrum is then given by

$$I^{\mathrm{CS}} = \left| \sum_{\alpha} (\mathbf{M}_{\alpha} \mathbf{e}_S)^* (\mathbf{M}_{\alpha} \cdot \mathbf{e}_L) \Psi_{\alpha}(t) \right|^2 \tag{A6}$$

with the complex function

$$\Psi_{\alpha}(t) = \int_{-\infty}^{+\infty} dt_1 \int_{-\infty}^{+\infty} dt_2 \, F_L(t_2) F_S^*(t - t_1) \times \exp[i\omega_S t_1 - i\omega_L t_2 - i(E_m - i\delta E_{\mathrm{hom},\alpha}/2) \times (t_1 - t_2)/\hbar] \, . \tag{A7}$$

The hot-luminescence component may be written as

$$I^{\mathrm{HL}} = \sum_{n=1}^{\infty} I^n(t) \tag{A8}$$

with the contribution of the nth order diagram

$$I^{(n)}(t) = \sum_{\alpha_1 \cdots \alpha_{n+1}} \bar{h}_{\alpha_1\alpha_2} \cdots \bar{h}_{\alpha_n\alpha_{n+1}} \left| (\mathbf{M}_{\alpha_1} \cdot \mathbf{e}_S)(\mathbf{M}_{\alpha_{n+1}} \cdot \mathbf{e}_L) \right|^2 \int_{-\infty}^{+\infty} dt_2 e^{(\delta E_{\mathrm{hom},\alpha_1} - \delta E_{\mathrm{hom},\alpha_2}) t_2/\hbar} |\Psi_{1,\alpha_1}(t, t_2)|^2 \times \int_{-\infty}^{t_2} dt_3 e^{(\delta E_{\mathrm{hom},\alpha_2} - \delta E_{\mathrm{hom},\alpha_3}) t_3/\hbar} \int_{-\infty}^{t_3} dt_4 \cdots \int_{-\infty}^{t_n} dt_{n+1} e^{(\delta E_{\mathrm{hom},\alpha_n} - \delta E_{\mathrm{hom},\alpha_{n+1}}) t_{n+1}/\hbar} |\Psi_{2,\alpha_{n+1}}(t_{n+1})|^2 \tag{A9}$$

and the abbreviations

$$\Psi_{1,\alpha_1}(t, t') = \int_{t'}^{\infty} dt'' F_S^*(t - t'') \times e^{i\omega_S t'' - i(E_{\alpha_1} - \frac{i}{2}\delta E_{\mathrm{hom},\alpha_1}) t''/\hbar} \tag{A10}$$

and

$$\Psi_{2,\alpha_{n+1}}(t') = \int_{-\infty}^{t'} dt'' F_L(t'') \times e^{-i\omega_L t'' + i(E_{\alpha_{n+1}} - \frac{i}{2}\delta E_{\mathrm{hom},\alpha_{n+1}}) t''/\hbar} . \tag{A11}$$

Equations (A6) and (A7) imply that the time dependence of the coherent component is determined by the homogeneous linewidth δE_{hom} of the exciton states. The hot luminescence depends through $\bar{h}_{\alpha_i\alpha_k}$ in addition on the pure dephasing rate w [Eqs. (A4) and (A9)]. From both quantities, with Eq. (1.1) the energy-relaxation time T_1 may be deduced.

In the case of resonant excitation of an ensemble of energetically split states, Eq. (A6) shows that the polarized coherent part of the scattered intensity oscillates with frequencies given by the energy differences of the states. Obviously the unpolarized hot luminescence [Eq. (A8)] does not show such oscillations indicating that the coherence is lost by phase relaxation. Therefore, *quantum beats* do occur only in the Raman scattered light. This provides the basis for the *experimental* discrimination between these processes as exemplified in the investigations reported here and represents a distinct advantage of time-resolved light scattering compared to other techniques by which only τ_{coh} can be obtained.

[1] S. Haroche, in *High Resolution Spectroscopy*, edited by K. Shimoda, Topics in Applied Physics Vol. 13 (Springer, Heidelberg, 1976), p. 253.

[2] E.B. Aleksandrov, N.I. Kaliteevski, and M.P. Chaika, Usp. Fiz. Nauk. **129**, 155 (1979) [Sov. Phys. Usp. **22**, 760 (1979)].

[3] A. Corney, Philos. Trans. R. Soc. London Ser. A **307**, 573 (1982).

[4] V. Langer, H. Stolz, and W. von der Osten, Phys. Rev. Lett. **64**, 854 (1990).

[5] E.O. Göbel, K. Leo, T.C. Damen, J. Shah, S. Schmid-Rink, W. Schäfer, J.F. Mueller, and K. Köhler, Phys. Rev. Lett. **64**, 1801 (1990).

[6] W. van der Poel, A. Severens, and C.T. Foxon, Opt. Commun. **76**, 116 (1990).

[7] B.F. Feuerbacher, J. Kuhl, R. Ecleston, and K. Ploog, Solid State Commun. **74**, 1279 (1990).

[8] H. Stolz, V. Langer, E. Schreiber, S. Permogorov, and W. von der Osten, Phys. Rev. Lett. **67**, 679 (1991).

[9] E.O. Göbel, M. Koch, J. Feldmann, G. von Plessen, T. Meier, A. Schulze, P. Thomas, S. Schmitt-Rink, K. Köhler, and K. Ploog, Phys. Status Solidi B **173**, 21 (1992).

[10] K.-H. Pantke and J.M. Hvam, Int. J. Mod. Phys. B **8**, 73 (1994).

[11] H. Stolz, Phys. Status Solidi B **173**, 99 (1992).
[12] W. von der Osten, V. Langer, and H. Stolz, in *Coherent Optical Interactions in Semiconductors*, Vol. 330 of *NATO Advanced Study Institute, Series B: Physics*, edited by R. Phillips (Plenum Press, New York, 1994).
[13] It has to be pointed out that our definition of the coherence time τ_{coh} and hence the homogeneous linewidth correspond actually to the upper state coherence time. As was shown in T. Takagahara, Phys. Rev. B **31**, 8171 (1985), in the case of excitonic polaritons the optical dephasing time T_2 agrees with the upper state coherence time.
[14] V.T. Agekyan, Phys. Status Solidi A **43**, 11 (1977).
[15] M. V. Klein, Phys. Rev. B **8**, 919 (1973).
[16] R.M. Martin and L.M. Falicov in *Light Scattering in Solids*, edited by M. Cardona, Topics in Applied Physics Vol. 8 (Springer, Heidelberg, 1975), p. 80.
[17] V. Langer, H. Stolz, W. von der Osten, D. Fröhlich, A. Kulik, and B. Uebbing, Europhys. Lett. **18**, 723 (1992).
[18] H. Stolz, in *Festkörperprobleme/Advances in Solid State Physics*, edited by U. Rössler (Vieweg, Braunschweig 1991), Vol. 31, p. 219.
[19] D. Fröhlich, A. Kulik, B. Uebbing, A. Mysyrowicz, V. Langer, H. Stolz, and W. von der Osten, Phys. Rev. Lett. **67**, 2343 (1991).
[20] D. Fröhlich, A. Kulik, B. Uebbing, V. Langer, H. Stolz, and W. von der Osten, Phys. Status Solidi B **173**, 31 (1992).
[21] P.Y. Yu and Y.R. Shen, Phys. Rev. B **12**, 1377 (1975).
[22] A.Z. Genack, H.Z. Cummins, M.A. Washington and A. Compaan, Phys. Rev. B **12**, 2478 (1975).
[23] J.S. Weiner and P.Y. Yu, Solid State Commun. **50**, 493 (1984).
[24] R.J. Elliott, Phys. Rev. **124**, 340 (1961).
[25] J.L. Birman and R. Berenson, Phys. Rev. B **9**, 4512 (1974); J.L. Birman, *ibid.* **9**, 4518 (1974).
[26] Y. Toyozawa, Prog. Theor. Phys. **20**, 53 (1958).
[27] D.Fröhlich and R. Kenklies, Phys. Status Solidi B **111**, 247 (1982).
[28] F. Bassani and L.C. Andreoni, in *Excited-State Spectroscopy in Solids*, Proceedings of the International School of Physics "Enrico Fermi," Course 96, Varenna, 1985, edited by U.M. Grassano and N. Terzi (North-Holland, Amsterdam, 1987).
[29] J. Aavicsoo, J. Lumin. **48&49**, 57 (1991).
[30] N. Caswell, J.S. Weiner, and P.Y. Yu, Solid State Commun. **40**, 843 (1981).
[31] N. Caswell and P.Y. Yu, Phys. Rev. B **25**, 5519 (1982).
[32] A. Mysyrowicz, D. Hulin, and A. Antonetti, Phys. Rev. Lett. **43**, 1123 (1979); **43**, 1275(E) (1979).
[33] M. Timme, E. Schreiber, H. Stolz, and W. von der Osten, J. Lumin. **55**, 79 (1993).
[34] J.S. Weiner, N. Caswell, P.Y. Yu, and A. Mysyrowicz, Solid State Commun. **46**, 105 (1983).
[35] V. Langer, Ph.D. thesis, Universität-GH Paderborn, 1992.
[36] V. M. Agranovich and V. L. Ginzburg, in *Crystal Optics with Spatial Dispersion and Excitons*, edited by V. M. Agranovich and V. L. Ginzburg, Springer Series in Solid State Sciences Vol. 42 (Springer, Berlin, 1984).
[37] H.-R. Trebin, H.Z. Cummins, and J.L. Birman, Phys. Rev. B **23**, 597 (1981).
[38] A. Goltzené and C. Schwab, in *Semiconductors. Physics of Non-tetrahedrally Bonded Elements and Binary Compounds I*, edited by O. Madelung, Landolt-Börnstein, New Series, Group III, Vol. 17, Pt. e (Springer, Berlin, 1983).
[39] M. Aihara, Phys. Rev. **A 18**, 606 (1978)